PROTEINS: Structure, Function, and Genetics 17:375–390 (1993)

A Comparison of ^{15}N NMR Relaxation Measurements With a Molecular Dynamics Simulation: Backbone Dynamics of the Glucocorticoid Receptor DNA-Binding Domain

Mats A. L. Eriksson, Helena Berglund, Torleif Härd, and Lennart Nilsson
Center for Structural Biochemistry (CSB), Karolinska Institute, NOVUM, S-141 57 Huddinge, Sweden

ABSTRACT **The rapid motions of the backbone of the DNA-binding domain of the glucocorticoid receptor (GR DBD) have been investigated using proton-detected heteronuclear NMR experiments on ^{15}N-labeled protein at pH 6.0 and with a 200 psec molecular dynamics simulation of hydrated GR DBD. The experimental data were interpreted in terms of a generalized order parameter (S^2) and an effective correlation time (τ_e) for the internal motion of each amide bond. A back calculation, using the same model, yielded the $\{^1H\}$–^{15}N nuclear Overhauser effects (NOEs) and the ^{15}N spin-lattice relaxation times (T_1) from the simulated data. The rapid motions of the backbone turned out to be rather limited and uniform throughout the protein, with a somewhat reduced mobility in the two major α-helical regions and a slightly enhanced flexibility for some residues in the first zinc coordinating region. The agreement between the experimental and simulated S^2-values was as good as quantitative for most of the residues, except for some residues that were subject to a more large-scale, and in the simulation thus poorly sampled, motion. Examples of such motions that were found in the simulation include jumps of the amide bond of Ile-487 between the charged oxygens of the side chain of Asp-485 and less distinct large scale motions for some of the residues in the extended regions, that were shown to give rise to noisy and/or fast decaying internal reorientational correlation functions. For these residues large differences in the simulated and experimental τ_e-values were found, indicating that motions on different time scales were dominating in the experimental and simulated values. The lower (<0.7) experimental NOEs for these residues could not be reproduced in the simulation and were shown to be a consequence of the lower τ_e-values estimated in the simulation. By combining information from the simulation and the experiment a more complete picture of the motions for these residues can be obtained as is illustrated with an estimation of the jump angle and jump frequency for the amide bond of Ile-487.** © 1993 Wiley-Liss, Inc.

Key words: transcription factors, zinc finger, generalized order parameter, effective correlation time, internal protein motions, Lipari–Szabo model, "model-free" approach

INTRODUCTION

Recent methodological advances in NMR spectroscopy have made it possible to investigate dynamic processes in proteins on various time scales using NMR relaxation measurements, and NMR structure determinations of small proteins are now often complemented by evaluations of rapid (picosecond) backbone dynamics using ^{15}N NMR relaxations measurements on ^{15}N-labeled protein samples.[1–7] Relaxation rates and heteronuclear cross-relaxation of a ^{15}N (or ^{13}C) nucleus depend on the values of the spectral density function, $J(\omega)$, at five characteristic frequencies. It has recently been shown that these spectral density function values can be determined in a series of experiments involving relaxation measurements of various coherences.[7] This procedure is often referred to as spectral density mapping.[7] However, a more common approach has been to measure only a limited set of relaxation parameters, typically ^{15}N T_1, T_2 relaxation rates and $\{^1H\}$–^{15}N cross-relaxation rates (NOEs), to characterize the extent of rapid backbone motions. The interpretation of relaxation data is in these cases often carried out using the so-called "model free" approach introduced by Lipari and Szabo,[8] in which restricted motions are described in terms of a limited set of parameters characterizing internal motions, normally a generalized order parameter (S^2) and an effective correlation time for internal motions (τ_e), in addition to the overall protein correlation time (τ_R). The advantage

Received June 29, 1993; revision accepted August 16, 1993.
Address reprint requests to Dr. Mats A.L. Eriksson, Center for Structural Biochemistry, Karolinska Institute, NOVUM, S-141 57 Huddinge, Sweden.

of the Lipari–Szabo approach is that it enables a "visualization" of the amplitude and time scale of internal motions and that it requires the experimental determination of fewer relaxation parameters than the spectral density mapping method. The drawback of the method is that an a priori assumption of the functional form of the spectral density is made in the interpretation. It has also been shown that extensions of the initial "model free" model can be made that account for more complex dynamic processes.[5,9]

Detailed information about internal protein dynamics can also be extracted from molecular dynamics (MD) simulations of hydrated proteins.[10,11] MD can provide information about the detailed nature of various dynamic processes including rapid processes which occur within a few picoseconds, to which NMR relaxation is insensitive even at high magnetic fields. Thus, one would like to use MD to get a more detailed picture of the motions than one can observe in the experiments. However, commonly quoted caveats with MD simulations have been that these are based on force fields which might not be sufficiently accurate and when simulating systems of the size that is required for most proteins, the limited length of the simulation run. Dynamic processes occurring on a slower (> 100 psec) time scale will then, for computational reasons, be poorly sampled, which can lead to inadequate information about such processes. It is therefore desirable to make detailed comparisons of experimental data with the results from an MD simulation, prior to drawing conclusions about the nature of a particular dynamic process. A good example of how simulated data and ^{15}N nuclear magnetic relaxation data can be combined is given in a 500 psec simulation of hydrated interleukin-1β,[10] where ^{15}N NMR relaxation measurements[5] suggested that the motion of some of the residues could be accounted for by a rapid motion within an axially symmetric cone and a slower motion consisting of jumps between two cones.[5,9] Since the exact physical nature of these motions was unresolved, MD-simulated data[10] revealed that most of these residues were exposed to the surface and some of the amide bonds of residues were shown to perform jumps between two distinct and well-defined orientations.

The question of experimental observation and determination of amplitudes of backbone motions versus the detailed nature of these motions applies to our studies of the structure and function of the glucocorticoid receptor DNA-binding domain (GR DBD). We recently studied the extent of picosecond mobility along the peptide backbone in this protein by measuring ^{15}N T_1 and ^{15}N $T_{1\rho}$ relaxation rates and $\{^1H\}$–^{15}N cross-relaxation rates in a uniformly ^{15}N-labeled GR DBD fragment.[4] Experimental data were in this case interpreted using the Lipari–Szabo approach.[8] The results led us to conclude that rapid backbone motions are uniform and restricted throughout the backbone of this protein. On the other hand, the MD simulation on the same protein fragment, presented here, suggests that a number of different distinct dynamic processes involving various peptide amides are present. One can, for instance, observe simple librational motions of amides within ordered secondary structures as well as more complicated processes involving rearrangement of hydrogen bonding, etc.

The structure of GR DBD (Fig. 1) has been determined in solution using NMR spectroscopy,[12,13] as well as in a dimeric complex with DNA using X-ray diffraction methods,[14] and consists of two subdomains (or motifs) that both have the general composition (abbreviations* that will be used for the regions are given in parentheses): zinc-coordinating domain (Zn_I and Zn_{II})–α-helix (α_I and α_{III})–extended region (ext_I and ext_{II}). The zinc ions are coordinating the sulfurs of four cysteins tetrahedrally (Fig. 1) and the two major helices (α_I and α_{III}) are oriented perpendicular to each other, forming the protein body. The second zinc coordinating domain, Zn_{II}, also contains a short piece of distorted α-helix (α_{II}). The two subdomains of GR DBD differ from each other both structurally and functionally; the first subdomain is involved in the DNA–GR DBD interaction, with some of the residues in the Zn_I region forming specific interactions with the phosphate groups of DNA and the α_I-helix is positioned in the major groove of DNA, with three residues forming specific contacts with the sequence-specific DNA, which GR DBD recognizes.[14–17] The second subdomain provides the entire dimerization interface where most of the intersubunit contacts are made by residues in the loop between Cys-476 and Cys-482, the "D-box"[17] (Fig. 1). Although there is good agreement between the crystallographically determined GR DBD structure[14] and the solution structure, determined with NMR,[12,13] there are still some ambiguities regarding the Zn_{II} region, which is well resolved in the crystal, but is less well defined in solution. Since this region is also poorly defined in the similar solution structure of the estrogen receptor DBD,[18] it has been speculated that this region is stabilized upon formation of the $(GR\ DBD)_2$–DNA complex.[14] The apparent disorder of this region in the solvated GR DBD might also be a reflection of the lack of nuclear Overhauser enhancement (NOE) connectivities, which is a recurrent problem in structure determination using NMR. Some structural elements give rise to only a few NOE constraints and this could in the worst case lead to a well-ordered region appearing less ordered. However, since no increased mobility was found in the Zn_{II} region in the previ-

*Throughout the text, the carbonyl oxygen will be abbreviated as O and the amide proton as NH.

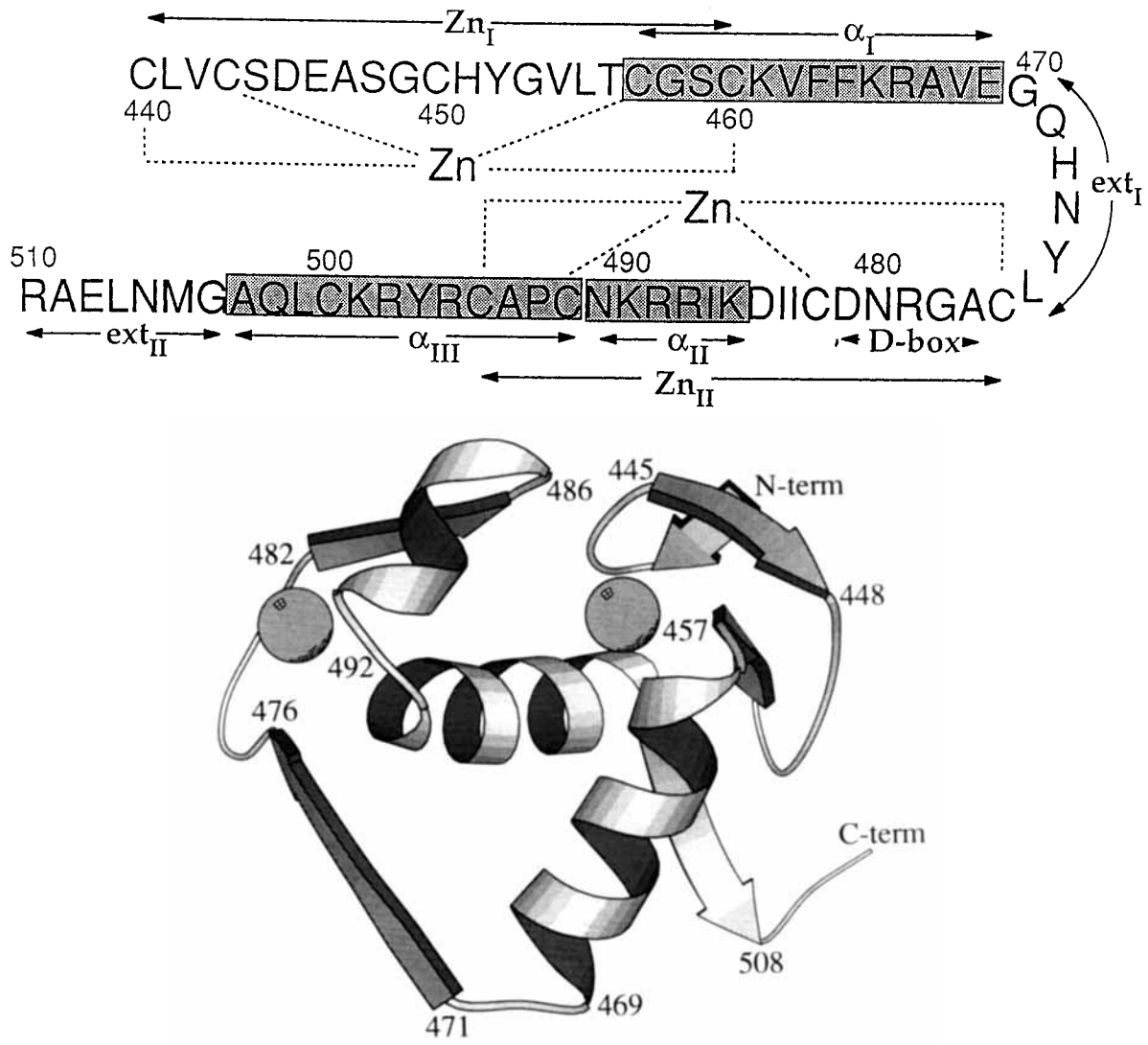

Fig. 1. The sequence of the rat glucocorticoid receptor DNA-binding domain (GR DBD). Abbreviations: Zn_I and Zn_{II}, first (N-terminal) and second zinc coordinating subdomains; α_I and α_{III}, first and second major α-helical subdomains; ext_I and ext_{II}, first and second extended regions; α_{II}, a short piece of a distorted α-helix in the Zn_{II} region. The α-helical segments are marked with boxes **(top)**. The crystal structure of GR DBD[14] is drawn in a ribbon representation[36] with the two zinc ions represented by hard spheres **(bottom)**.

ously mentioned ^{15}N NMR relaxation study,[4] this suggests that the lack of NOE connectivities in the structure gives rise to the apparent disorder.

In the present paper we will compare the results of proton-detected heteronuclear ^{15}N NMR relaxation measurements on uniformly ^{15}N-labeled GR DBD at pH 6.0 with a 200 psec molecular dynamics simulation of the same protein immersed in a 30 Å radius sphere of water molecules. The major objectives are the following: (1) To examine simulated correlation functions for peptide amide motions to determine if these are adequately described using the model free approach. (2) To quantitate order parameters and effective correlation times (S^2 and τ_e, respectively) for such motions and compare these to experimentally determined values. (3) To examine the nature of internal motions that cannot be exctracted from NMR relaxation measurements, analyzed within the Lipari–Szabo formalism.

MATERIALS AND METHODS

Theoretical Background

The motions of a peptide amide, resulting in ^{15}N relaxation and ^{1}H–^{15}N cross-relaxation can be described by the autocorrelation function

$$C(t) = \langle P_2[\mathbf{h}_i(0)\mathbf{h}_i(t)]\rangle \quad (1)$$

where $P_2 = (3x^2-1)/2$ is the second-order Legendre polynomial and $\mathbf{h}_i$ is a unit vector pointing along the

amide bond of residue i. The general shape of $C(t)$ is often a rapid initial decay, complete after a few picoseconds, to a plateau value due to internal motions on a picosecond time scale, followed by a much slower decay due to the overall tumbling motion, that occurs on a nanosecond time scale.[19] In the "model free" formalism adopted by Lipari and Szabo,[8] the correlation function for an isotropically tumbling molecule is, assuming that the overall and internal motions are independent,

$$C(t) = C_{2i}(t)e^{-t/\tau_R} \quad (2)$$

where τ_R is the overall correlation time for the molecular and the correlation function, $C_{2i}(t)$, for the internal motions which with this formalism can be written as

$$C_{2i}(t) = S^2 + (1 - S^2)e^{-t/\tau_e}. \quad (3)$$

S^2 is interpreted as the generalized order parameter and is a model-independent measure of the degree of spatial restriction of the internal motion. S^2 ranges from 1 for no internal motion at all to 0 for a completely unrestricted motion where all orientations of the amide vector are equally probable. τ_e is the effective correlation time for the internal motion. S^2 can be determined from the limiting value of $C_{2i}(t)$:

$$S^2 = \lim_{t\to\infty} C_{2i}(t) = \lim_{t\to\infty} < P_2[\mathbf{h}_i'(0)\mathbf{h}_i'(t)] > \quad (4)$$

where $\mathbf{h}_i'$ is the molecule fixed frame unit vector along the amide bond of residue i.

Relaxation of an amide ^{15}N is dominated by two mechanisms[20]: dipole–dipole coupling to its directly bound hydrogen and chemical shift anisotropy. The NMR relaxation parameters are functions of the spectral density $J(\omega)$, which is the Fourier transform of the correlation function at certain characteristic frequencies. Ignoring cross-correlation, the spin lattice relaxation time T_1 and the heteronuclear $\{^1H\}$–^{15}N NOE can be expressed as[1]

$$\frac{1}{T_1} = d^2[J(\omega_A - \omega_X) + 3J(\omega_X) + 6J(\omega_A + \omega_X)] + c^2J(\omega_X) \quad (5)$$

$$NOE = 1 + \frac{T_1\gamma_A d^2}{\gamma_X}[6J(\omega_A + \omega_X) - J(\omega_A - \omega_X)] \quad (6)$$

with $d^2 = 1/10\ [\gamma_A\gamma_X\hbar\mu_0/4\pi]^2 <1/r_{AX}^3>^2$ and $c^2 = 2/15[\omega_X(\sigma_\parallel - \sigma_\perp)]^2$, and where A = ^1H, X = ^{15}N, and γ_i and ω_i are the gyromagnetic ratio and Larmor frequency of spin i, respectively. μ_0 is the permeability of vacuum, r_{AX} is the internuclear ^1H–^{15}N distance (1.02 Å) and $\sigma_\parallel - \sigma_\perp$ (= −160 ppm) is the difference between the parallel and perpendicular components of the ^{15}N chemical shift tensor.[21]

Assuming that the overall rotational motion is isotropic, the spectral density can be written[8]:

$$J(\omega_i) = \frac{S^2\tau_R}{[1 + (\omega_i\tau_R)^2]} + \frac{(1 - S^2)\tau}{[1 + (\omega_i\tau)^2]} \quad (7)$$

where $1/\tau = (1/\tau_R) + (1/\tau_e)$ and τ_R is the overall rotational correlation time of the protein. It should be noted that this expression is exact even if $C_{2i}(t)$ is multiexponentially decaying, as long as the rates are in the extreme narrowing limit.[8]

Experimental

Sample preparation

The fragment L439-Q520 of the rat glucocorticoid receptor was expressed, ^{15}N-labeled, and purified as described previously.[4] NMR measurements were performed on a 0.9 mM sample of GR DBD in 250 mM NaCl, 20 mM phosphate, and 2 mM DTT at pH 6.0. The NMR tube containing the sample was repeatedly flushed with nitrogen in order to minimize the amount of dissolved oxygen in the sample.

^{15}N NMR relaxation measurements

Two-dimensional heteronuclear correlation spectra were recorded on a Varian Unity 600 MHz spectrometer at a temperature of 299 K. T_1 relaxation times and $\{^1H\}$–^{15}N NOEs were measured and processed as discussed in Berglund et al.[4] The T_1 relaxation rate constants and $\{^1H\}$–^{15}N NOEs were calculated from peak heights in heteronuclear correlation spectra. Seven two-dimensional T_1 inversion recovery spectra were recorded with relaxation periods ranging from 9 to 2,991 msec and peak heights measured in these spectra were fitted to the functional form $Ae^{(-t/T_1)} + B$ using nonlinear least-squares curve fitting. Heteronuclear NOEs, (I/I_0), were determined from ratios between peak heights in spectra recorded with and without heteronuclear NOE. Uncertainties in the measured peak heights were estimated from the baseline noise level. Errors in the derived T_1 values were estimated standard deviations derived from the covariance matrix from the parameters obtained from the least-squares fitting process. From uncertainties in measured peak heights, errors in the measured NOE values were derived. The experimental values of S^2 and τ_e were determined by minimization of the expression $\chi^2 = (NOE_{calc} - NOE_{exp})^2/(\sigma_{NOE})^2 + (T_{1calc} - T_{1exp})^2/(\sigma_{T_1})^2$, where NOE_{exp} and T_{1exp} are the experimentally determined values of T_1 and NOE, and NOE_{calc} and T_{1calc} are calculated from Eqs. (5) and (6). We used the experimental value of τ_R, which has been determined on a similar sample of GR DBD[4] and where a value of $\tau_R = 6.3 \pm 0.1$ nsec was obtained. Uncertainties in the determined S^2 and τ_e were estimated from Monte Carlo simulations.

Simulation details

The parameterization of the zinc atoms and the MD simulation will be discussed in full detail to-

gether with other aspects of the structure and dynamics of GR DBD as well as its hydration.[22] In this paper we will therefore give a more summarized description of the simulation.

The zinc atoms were covalently bonded to the cystein sulfurs in a tetrahedral coordination sphere (Fig. 1). Partial charges and bond/angle parameters for the atoms in the vicinity of the zinc atoms were incorporated in the force field "par_ all22_ prot_ b2" of the program package CHARMM,[23] version 22 (Harvard University, Department of Chemistry, Cambridge, MA) by using MNDO[24–26]/ESP[27] calculations with the program package MOPAC.[28] The coordinates of the fragment Cys-440–Arg-510 of the DNA-binding domain of the glucocorticoid receptor were taken from the $(GR\ DBD)_2$–DNA complex, determined with X-ray crystallography[14] and the hydrogen atoms were positioned with the CHARMM subroutine HBUILD.[29]

The protein was immersed in a sphere of radius 30 Å with TIP3P–water.[30] To achieve electroneutrality, the four water molecules with the lowest electrostatic potential at the oxygen were replaced with chloride ions. The water molecules interacted with a "deformable boundary force,"[31] arising from mean field interactions of water molecules beyond 30 Å. In the region between 27 and 30 Å (the buffer region) the molecules interacted with a stochastic heat bath of 300 K, via random fluctuating forces and dissipative forces.[32] The ordinary MD equations of motion were applied for water molecules inside 27 Å. We used a timestep of 2 fsec and the SHAKE[3] algorithm constrained the bonds. The system was equilibrated for 40 psec, followed by a 200 psec production run. We investigated the time evolution of the root mean square deviation of the backbone from the initial (crystal) structure to decide whether the system had been sufficiently equilibrated; when this curve had flattened out, we started the production run.

Calculation of the S^2, τ_e, *NOE, and* T_1*-values from the simulation*

We evaluated the generalized order parameters, S^2 by estimating the plateau value of the calculated autocorrelation function given by Eq. (1). A simple error estimate of S^2 was provided from the upper and lower bounds of the plateau, due to the noise or oscillations of $C_{2i}(t)$.

Prior to the calculation of the correlation function $C_{2i}(t)$, the overall motion of the molecule was removed by rotating the coordinate sets to fit the initial structure of GR DBD as close as possible. This was done by minimizing the mass weighted root mean square deviation of the backbone between the initial and the actual structure. The $C_{2i}(t)$s were found to differ slightly, but systematically for each residue if this rotation was not carried out, suggesting that the molecule had rotated as a whole during the stimulation. We therefore calculated the $C_2(t)$ for the unrotated unit vector connecting the two zinc ions of the protein and fitted the curve to an exponentially decaying function:

$$C_2(t)_{Zn\rightarrow Zn} = e^{-t/\tau_R} \tag{8}$$

where τ_R is the overall rotational time of the protein; this resulted in a τ_R of 4 nsec.

The effective correlation time for the internal motion, τ_e, was estimated for each residue according to[8]

$$\tau_e = \frac{1}{(1 - S^2)} \int_0^\infty [C_{2i}(t) - S^2]\, dt \tag{9}$$

and an error estimation of τ_e was obtained by recalculating Eq. (9) with the upper and lower bounds of S^2.

The most straightforward way of calculating the spectral densities appearing in Eqs. (5)–(6) would have been a direct Fourier transform of the correlation functions:

$$J(\omega) = \int_0^{t'} C(t) \cos(\omega t)\, dt \tag{10}$$

where t' is correlated time. Unfortunately, with a t' of 100 psec, the lowest frequency would be 10^4 MHz, which is 2–3 orders of magnitude too large for the frequencies measured in the NMR experiment (~ 10–600 MHz). To estimate these frequencies would thus require the simulated time to be 100–1000 times longer (20–200 nsec). We therefore have to evaluate the $\{^1H\}$–^{15}N NOEs and T_1-values using Eqs. (5)–(7). The disadvantage with this procedure is the need of introducing the order parameters (S^2), estimating them from the $C_{2i}(t)$s and assuming that Eq. (4) is valid for these S^2-values. However, no assumption has to be made about the shape of the $C_{2i}(t)$s, since τ_e is evaluated using Eq. (9).

RESULTS AND DISCUSSION

The Reorientational Correlation Functions

The correlation functions for internal motions, $C_{2i}(t)$, differ significantly but not systematically in shape from residue to residue and can roughly be divided into three categories: (1) The plateau value, after the initial rapid decay, extends throughout the correlated time, which was 100 psec. This shape of the correlation functions gives good (if the functions are not too noisy) estimates of S^2 and was found for most of the residues. (2) The plateau extends for a shorter time (< 60 psec) and $C_{2i}(t)$ starts decaying again. This behavior was found for some residues in the C-terminal of the α_I region, ext_I, α_{II}, and in the α_{III} region and could indicate that when the $C_{2i}(t)$ starts decaying again, the reorientation of the amide bond is determined by some large scale motion of the protein. One example of such a large scale motion is infrequent jumps of the amide bond between two preferred orientations, as will be discussed in more

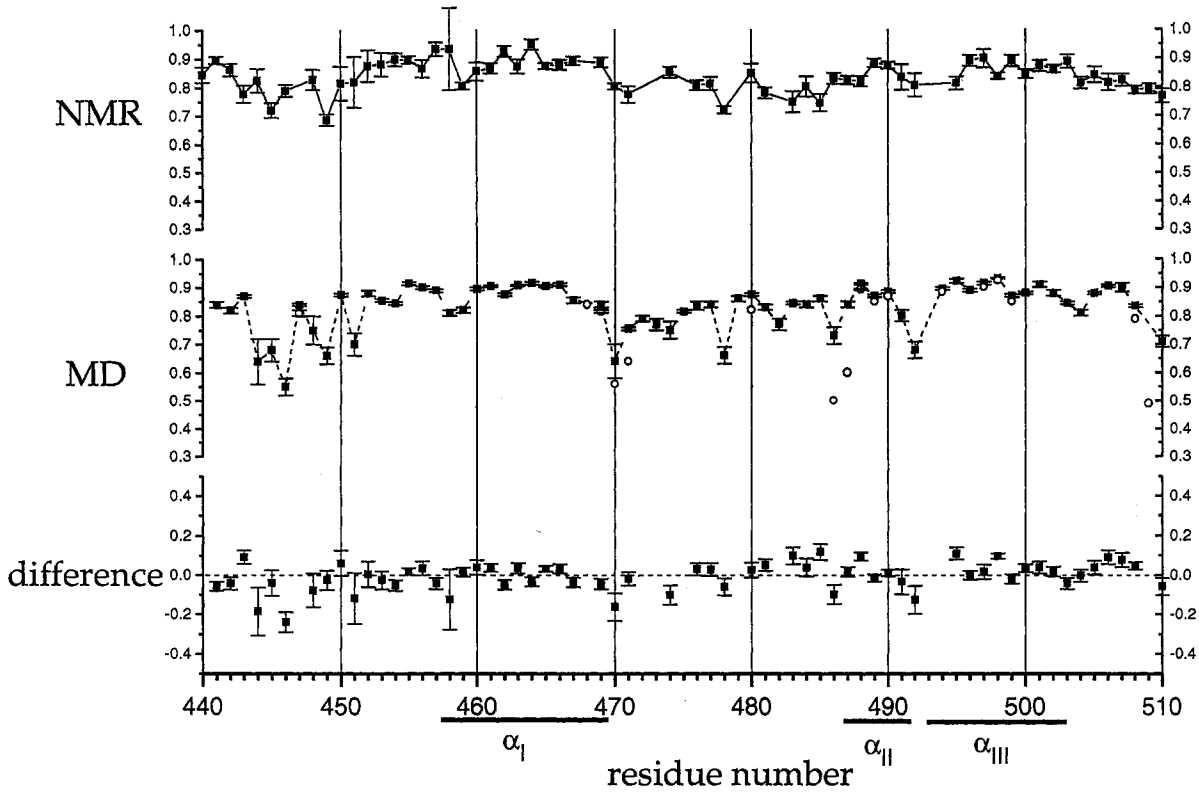

Fig. 2. Generalized order parameters (S^2) of the amide bonds of the backbone. **Top,** experimental; **middle,** simulated; **bottom,** difference between simulated and experimental values.

detail below. In Figure 2 (middle) the final values (at 100 psec correlated time) are shown as circles for this category of $C_{2i}(t)$s, together with the plateau value (shown as squares). (3) For the final category of $C_{2i}(t)$s, no plateau value is reached within the 100 psec of correlated time. In fact, the only residue which showed this behavior was Ala-509 and the final value is shown as a circle in Figure 2. This could either indicate that the plateau value will be reached on a longer time scale than 100 psec or that the reorientation of the amide bond is too complicated to be described by a rapid motion superimposed on a much slower, overall rotational motion. Typical examples of correlation functions for the first two categories and $C_{2i}(t)$ for Ala-509 are shown in Figure 3.

Generalized Order Parameters

A general feature of the amide bonds of GR DBD is the uniform mobility over the entire protein, which is probably due to the compactness of GR DBD, with only short extended regions and a network of hydrogen bonds between carbonyl oxygens and amide hydrogrens spanning most of the residues in the protein.[12–14] This uniform mobility of the amide bonds is clearly seen from the average experimental and simulated order parameters for the different regions in the protein (Table I). Averages slightly higher than the total are found for the two major helices (α_I and α_{III}) and are a result of the structuring effect of the hydrogen bonds between a carbonyl oxygen and an amide hydrogen four residues ahead along the helix. Regions with higher mobility, as indicated by average S^2-values lower than the average over the entire protein, are the ext_I and the "D-box" region, which is involved in the dimerization upon formation of a complex with DNA.[13,14] In a refinement of the NMR structure of DBD in solution (Baumann et al., in press, in *Biochemistry*), this region was on average found to be oriented differently compared to the crystal structure and RMSD-values between the 24 resulting structures were very high in this region. These results are supported by the MD simulation, since the fluctuations of the backbone show a local maximum for the residues in this region.[2] Slightly more mobile residues are also found in the middle of the Zn_I region (Fig. 2). The motion of this part of the protein is rather concerted as seen in an analysis of the cross-correlation coefficients for displacements of the backbone atoms[22] and the slight decrease of the order parameters is therefore probably due to a motion of this region as a whole.

Regarding the correlation between the secondary

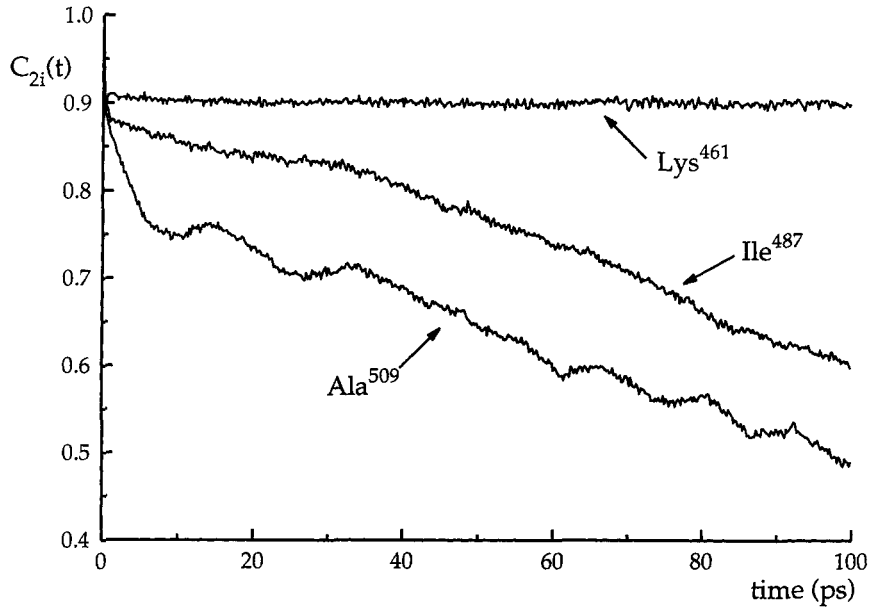

Fig. 3. Three typical categories of the $C_{2i}(t)$s. Lys-461 is representative of category 1, Ile-487 of category 2, and Ala-509 is the only residue of category 3 (see text).

TABLE I. Averaged S^2 Over Certain Regions*

	S^2	
Subdomain	Simulated	Experimental
Zn_I	0.80 (0.10)	0.84 (0.07)
α_I	0.88 (0.04)	0.89 (0.04)
ext_I	0.77 (0.06)	0.81 (0.03)
Zn_{II}	0.83 (0.07)	0.81 (0.05)
"D-box"	0.81 (0.09)	0.79 (0.06)
α_{II}	0.84 (0.07)	0.84 (0.03)
α_{III}	0.88 (0.07)	0.86 (0.03)
ext_{II}	0.84 (0.07)	0.81 (0.03)
Total	0.83 (0.08)	0.84 (0.06)

*The numbers in parentheses are the spread (standard deviation) around the average. The simulated values have been omitted for residues where no experimental data were available.

structure and the order parameters, different results have been obtained for various proteins, investigated with ^{15}N NMR spectroscopy.[1-4,6] In a study of the protein staphylococcal nuclease,[1] no such correlation was found on the time scale (10^{-8}–10^{-12} sec) relevant for T_1-values and NOEs, with averaged order parameters of 0.86 for all regions of the protein. However, T_2-values, which also are sensitive to motions on a millisecond time scale,[1] indicated a possible correlation between the mobility of an amide bond and its secondary structure. In ^{15}N NMR relaxation studies of the ribonuclease H domain of HIV-1,[2] lower values of the order parameters were found in loops between α-helical and β-structured regions. In a ^{15}N NMR experiment on calbindin D_{9K},[3] order parameters around 0.85 (± 0.04) were found for the helical regions, whereas S^2-values as low as 0.59 (± 0.23) were obtained for the linker region of this protein. Unusually low S^2-values in turns and loops connecting the β-strands of interleukin-1β[5] were obtained, whereas no apparent correlation between the secondary structure and the S^2-values was found in human ubiquitin.[6] However, the order parameters for residues, which amide groups/carbonyl oxygens were involved in intramolecular hydrogen bonds, were found to be higher (average S^2 = 0.80 ± 0.06) than for backbone atoms, not participating in any hydrogen binding[6] (average S^2 = 0.69 ± 0.06).

The agreement between our experimentally estimated order parameters and the simulated is quite good, with a few exceptions (see Fig. 2, bottom), where the difference is plotted. Some of the disagreements can be explained by jumps of an amide hydrogen/carbonyl oxygen between two nearby carbonyl oxygens/amide hydrogens during the simulation run. The carbonyl oxygen of residue Asp-485 has jumped between the amide protons of Ser-444 and Arg-489 (Fig. 4, top) and one of the N-terminal amide protons of Cys-440 has jumped between the carbonyl oxygens of Glu-446 and Asp-445 (Fig. 5). Since these jumps occur only a few times in 200 psec, the statistics of the $P_2(t)$s of the residues involved in these jumps is rather poor, yielding quite noisy curves. (Note that in the case of a jumping carbonyl oxygen, the amide bond of the *following* residue will flip concertedly, because of the partial double bond character of the peptide bonds.[34]) Ser-444, Glu-446, and Lys-486 are all too low compared to the experimental estimated values, and to verify that these

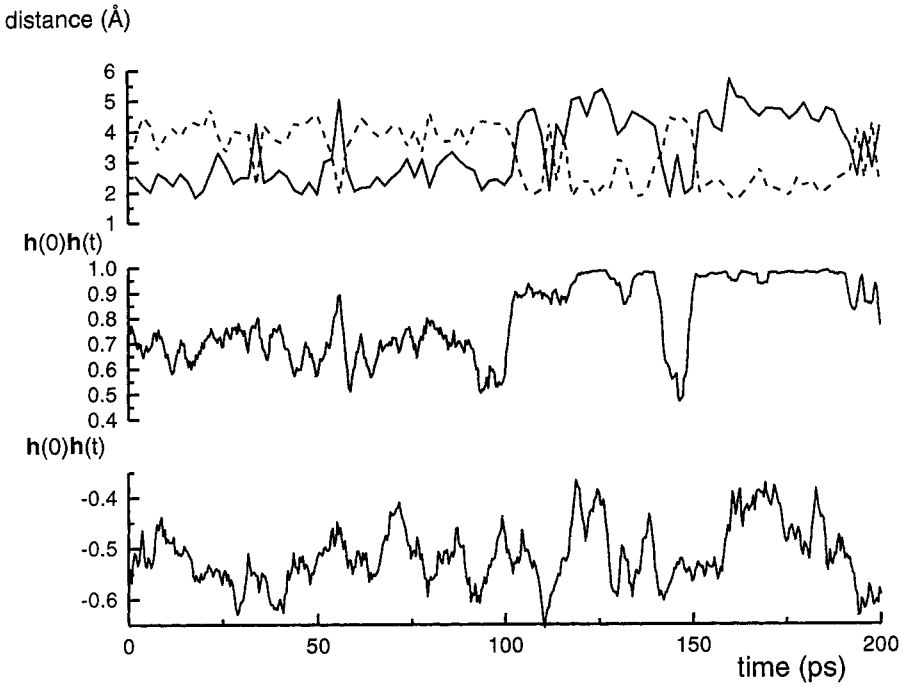

Fig. 4. **Top:** Distance between the carbonyl oxygen of Asp-485 and the amide proton of Ser-444 (solid line) or the amide proton of Arg-489 (dashed line) during the simulation. Two lower: scalar product of the unit vector along the amide bond **h**(0)**h**(*t*), during the time evolution of the simulation for Lys-486 **(middle)** and for Ser-444 **(bottom)**.

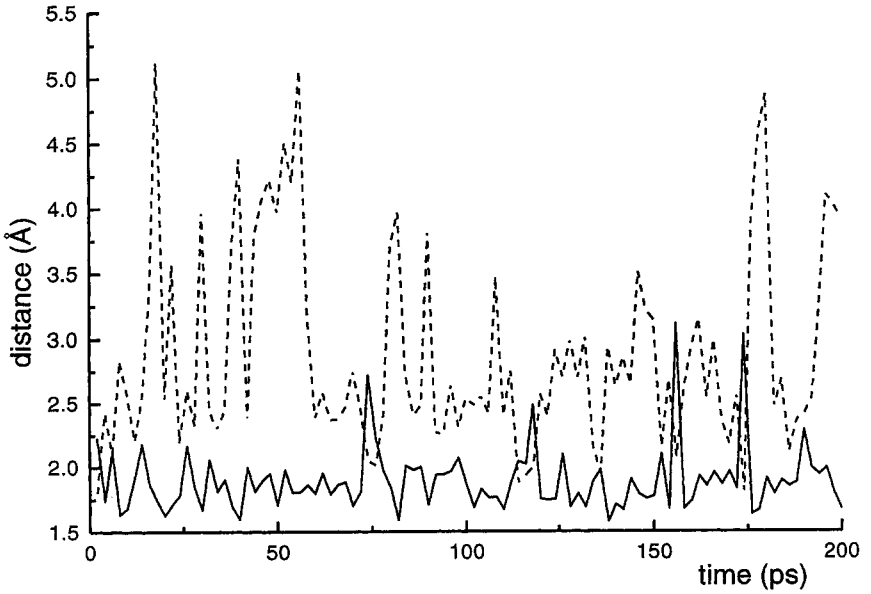

Fig. 5. Distance between one of the N-terminal amide protons of Cys-440 and the carbonyl oxygen of Glu-446 (solid line) or the carbonyl oxygen of Asp-445 (dashed line) during the simulation.

jumps are causing the noise in the $C_{2i}(t)$s, the order parameters were recalculated for residues Ser-444, Lys-486, and Arg-489 for shorter time periods, during which no jump occurred. The first time period was chosen between 0 and 30 psec, where Ser-444 is hydrogen bonded to Asp-485 and the second time period was chosen between 150 to 180 psec, where instead Arg-489 is the hydrogen donor. The recalculation resulted in correlation functions with a distinct plateau value and the results, together with

TABLE II. Estimated S^2-Values for Some Selected Residues Over Shorter Time Periods

Residue	0–30 psec	150–180 psec	0–200 psec	Experimental
Ser-444	0.84 (±0.03)	0.86 (±0.05)	0.64 (±0.08)	0.83 (0±0.04)
Lys-486	0.87 (±0.02)	0.91 (±0.01)	0.73 (±0.03)	0.83 (±0.02)
Arg-489	0.87 (±0.01)	0.91 (±0.01)	0.87 (±0.01)	0.88 (±0.01)
		60–90 psec		
Ile-487	0.90 (±0.01)	0.89 (±0.01)	0.84 (±0.01)	0.83 (±0.02)
		120–200 psec		
Gly-470		0.83 (±0.02)	0.64 (±0.06)	0.80 (0±0.01)

the order parameter estimated over the whole production run and the experimental values, are shown in Table II. The values for the two hydrogen donating residues, Ser-444 and Arg-489, are now in agreement with experiment, whereas S^2 of Lys-486 gives a slightly too high estimate.

The changed orientation of the amide bone of Lys-486 during these jumps is clearly seen when plotting the scalar product $\mathbf{h}(0)\mathbf{h}(t)$ between $\mathbf{h}(0)$, the unit vector along the amide bond of Lys-486 at the start of the production run, and $\mathbf{h}(t)$ during the time evolution of the simulation (Fig. 4, middle). This scalar product is the cosine of the angle between the initial orientation and the orientation at time t of the amide bond. The correlation coefficient between the time evolution of the distance Ser-444–NH–Asp-485–O and $\mathbf{h}(0)\mathbf{h}(t)$ for the amide bond of Lys-486 was 0.81. The orientation of the amide bond of Ser-444 is less affected by the jumps of Asp-485–O, but a slight correlation (correlation coefficient 0.48) is seen between the distance Ser-444–NH–Asp-485–O and $\mathbf{h}(0)\mathbf{h}(t)$ for the amide bond of Ser-444 (Fig. 4, bottom). The occasional hydrogen bonding of Asp-485–O to Ser-444–NH acts more as a perturbation of the orientation of the amide bond of Ser-444. The orientation has changed about 120° during the whole simulation with respect to the inital orientation and has probably occurred due to better coordination with Asp-485–O.

The decay of $C_{2i}(t)$ for the amide bond of Ile-487 to a very low value at 100 psec correlated time (Fig. 3) could be understood with a similar analysis: In the crystal structure the amide proton of this residue is hydrogen bonded to Asp-485–$O_{\delta 1}$, i.e., one of the charged oxygens of the side chains. This is also the case in the first half of the production run, but during the latter half of the simulation, the amide proton of Ile-487 is instead hydrogen bonded to the other charged oxygen, Asp-485–$O_{\delta 2}$ (Fig. 6, top). Plotting $\mathbf{h}(0)\mathbf{h}(t)$ for the amide bond of Ile-487 during the time evolution of the simulation (Fig. 6, bottom) shows the correlation between the distance Asp-485–$O_{\delta 1}$–Ile-487–NH and $\mathbf{h}(0)\mathbf{h}(t)$ for the amide bond of Ile-487 (correlation coefficient −0.72). Recalculating $C_{2i}(t)$ of Ile-487 for a simulated period where no such jump occurs (0–30 and 60–90 psec), the curve decays to a plateau value of 0.89 (± 0.01, see Table II), that reaches troughout the correlated time, showing that these jumps cause the rapid final decay of Ile-487. In a 500 psec simulation of the protein interleukin-1β,[10] similar results were obtained. Residues that, with ^{15}N NMR relaxation experiments,[5] were found to perform motions occurring on a time scale slower than the fast motion common to all residues, gave rise to poor statistics of the $C_{2i}(t)$ correlation functions, caused by the poor sampling of these slower motions.

For the residues that are performing jumps, as discussed above, it would have been natural to use an extended[9] form of the Lipari and Szabo model,[8] where the correlation function for the internal motions of the residue is divided into a fast and a slower decaying component with effective correlation times τ_f and τ_s, respectively, according to[9]

$$C_{2i}(t) = S^2 + (1 - S_f^2)e^{t/\tau_f} + (S_f^2 - S^2)e^{t/\tau_s}. \quad (11)$$

This division requires τ_f and τ_s to differ by 1–2 orders of magnitude for the motions to be independent of each other.[9] The total generalized order parameter S^2 can then be decomposed according to

$$S^2 = S_f^2 S_s^2 \quad (12)$$

where S^2_f and S^2_S are the generalized order parameter for the faster and slower motions, respectively. A schematic illustration of this kind of correlation function is shown in Figure 7.

In a simple model,[5] which apparently would be appropriate for the residues Lys-486 and Ile-487, the slower motion consists of jumps between two discrete orientations (state i and j), differing by an angle φ_s, and the faster motion accounts for axially symmetric diffusion within cones centered around the two states (i and j). With this model, it can be shown[35] that S^2_S can be written as

$$S_s^2 = \sum_{k=i}^{j} \sum_{l=j}^{i} p_{eq}(k)p_{eq}(l)P_2(\cos\varphi_{kl}) \quad (13)$$

where $p_{eq}(i)$ and $p_{eq}(j)$ are the probabilities for the residency in state i and j.

To acquire reliable estimates of $p_{eq}(i)$ and $p_{eq}(j)$ would require considerably (~100 times) longer sim-

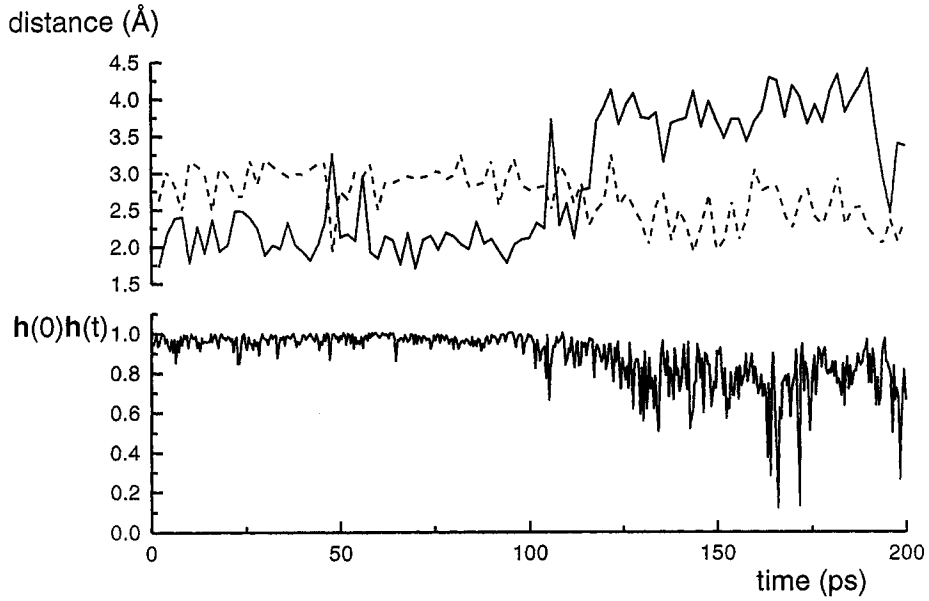

Fig. 6. **Top:** Distance between the amide proton of Ile-487 and Asp-485–$O_{\delta 1}$ (solid line) or Asp-485–$O_{\delta 2}$ (dashed line) during the simulation. **Bottom:** scalar product of the unit vector along the amide bond **h**(0)**h**(*t*), during the time evolution of the simulation for Ile-487.

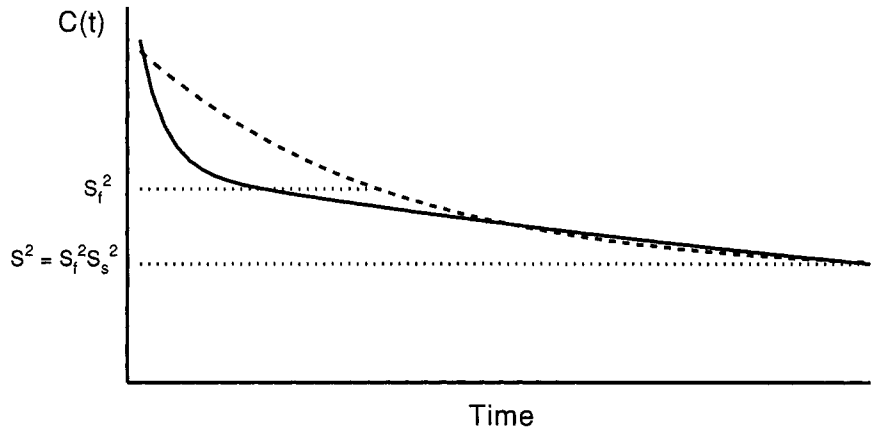

Fig. 7. A schematic illustration of the internal correlation function $C_{2i}(t)$ that can be approximated as a double exponentially decaying function [Eq. (11), solid line]. The dashed line is the shape of $C_{2i}(t)$ that will be assumed, adopting the "model-free" model [Eq. (3)] by Lipari and Szabo.[8]

ulation run and the estimation of S^2_S and τ_s must therefore be ruled out in the MD simulation. However, to illustrate how simulated and experimental data can be used together, a rough estimate of S^2_S for Ile-487 can be made: the estimated order parameter, that was obtained from the correlation function during times where no jump occurred, can be taken as an estimate of $S^2_f = (0.89 + 0.90)/2 = 0.895$ (Table II) and the experimentally estimated S^2 would, within the Lipari–Szabo approach, be a measure of the "total" generalized order parameter,[9] i.e., of the product $S^2_S S^2_f$ [Eq. (12)]. With $S^2 = 0.83$ (± 0.02) we then obtain $S^2_S = 0.83/0.895 = 0.93$ (± 0.02). If we, for simplicity, assume that both sites are equally probable, i.e., that $p_{eq}(i) = p_{eq}(j)$, Eq. (13) reduces to $S^2_S = (1 + 3\cos^2 \varphi_S)/4$ and the angle φ_S between the two orientations would be approximately 17°. This can be compared with results from a ^{15}NMR experiment[5] on the protein interleukin-1β, where jump angles ranging from 15° to 69° were obtained, using this extended model.

The underestimated order parameters of Gly-470 and the rapid decay of Gln-471 during the end of the correlated time (shown as a circle in Fig. 2) are clarified when calculating **h**(0)**h**(*t*) for their amide bonds (Fig. 8). During the first 50 psec of production run the orientation of the amide bond of Gly-470 (Fig. 8, top) fluctuates rather heavily, but oscillates closer

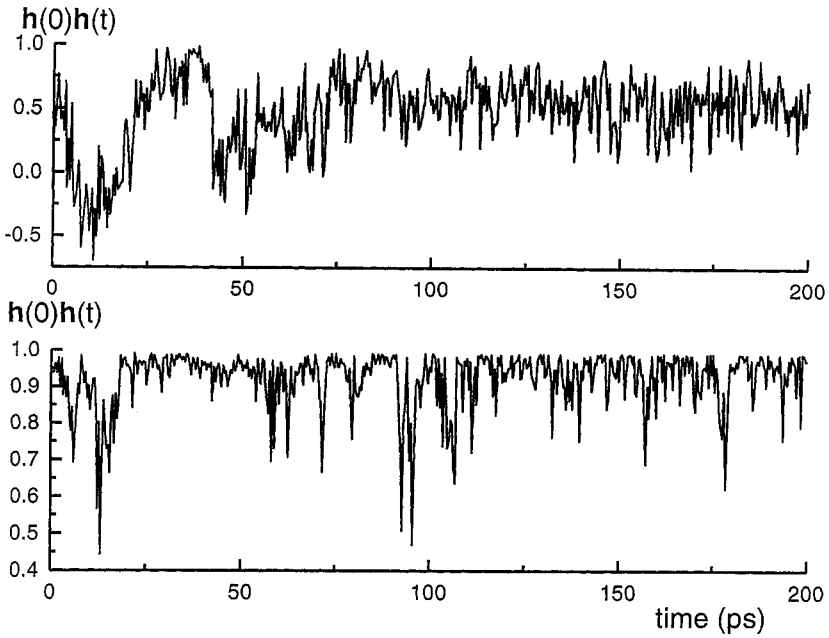

Fig. 8. Scalar product of the unit vector along the amide bond **h**(0)**h**(*t*), during the time evolution of the simulation for Gly-470 **(top)** and for Gln-471 **(bottom).**

to the original orientation in the later part of the simulation run. The rapid final decay of Gln-471 (shown as a circle in Fig. 2) is a result of the sudden changes of the orientation of the amide bond of Gln-471 (Fig. 8, bottom). The behavior of these residues is not surprising, considering the fact that they are in the ext_I region and probably undergo more large scale motions, which have been poorly sampled in the simulation. When $C_{2i}(t)$ was recalculated for the last 80 psec for Gly-470 and Gln-471, the correlation functions decayed rapidly to a plateau value with no further decay. The estimated order parameters of Gly-470 for this recalculation (Table II) was then in good agreement with the experimental value.

Effective Correlation Times for Internal Motions

The estimation of τ_e is very sensitive to the accuracy of the S^2-values and the statistical uncertainties are therefore large, sometimes as large as the estimated τ_e itself. A more accurate estimate of τ_e would require a considerably longer simulation run. Many of the experimentally estimated τ_e-values, which also have very large statistical uncertainties, are an order of magnitude larger than the simulated. The discussion of these values will therefore be more qualitative and in Figure 9 the error bars have been omitted for better visualization. Generally, for the residues belonging to category 1, the experimental and simulated τ_e-values are in reasonable agreement, whereas for most of the residues belonging to category 2, the experimental τ_e-values are much larger than the simulated. Since the "model-free" approach[8] was applied to interpret the experimental data, residues performing motion on a longer time scale will be approximated as the dashed line in Figure 7, and in terms of an integral over the correlation function [Eq. (9)] it is easily seen that this model will give rise to high τ_e-values for these residues. Since the length of the simulation run allows us to properly sample only the most rapid motions, as discussed above, the simulated correlation functions will essentially sample motions corresponding to the first plateau value in Figure 7 for these residues and the second, slower motions such as jumps, will act more as a perturbation on the $C_{2i}(t)$s.

Another interesting observation is that some residues, which have very large differencies in simulated and experimentally estimated τ_e-values (Fig. 9, bottom), such as Gly-459, Asn-474, Asn-491, and Arg-510, belong to category 1 in the simulation. This could probably be rationalized since for these residues, the slower motion giving rise to such high experimental τ_e-values occurs on a time scale which will not be sampled at all within the simulated time. In this case, all sampling of the motion will be done on the rapid initial decay (i.e., to the first plateau in Fig. 7) and no "perturbation" from the slower motions, leading to noisy correlation functions, will be seen.

Thus, in spite of the large statistical uncertainties in both the simulated and experimental τ_e-values, it is clear that they give some insight into the kinds of motions that a residue is involved in. Generally, for residues where experimental τ_e-values are fast, and

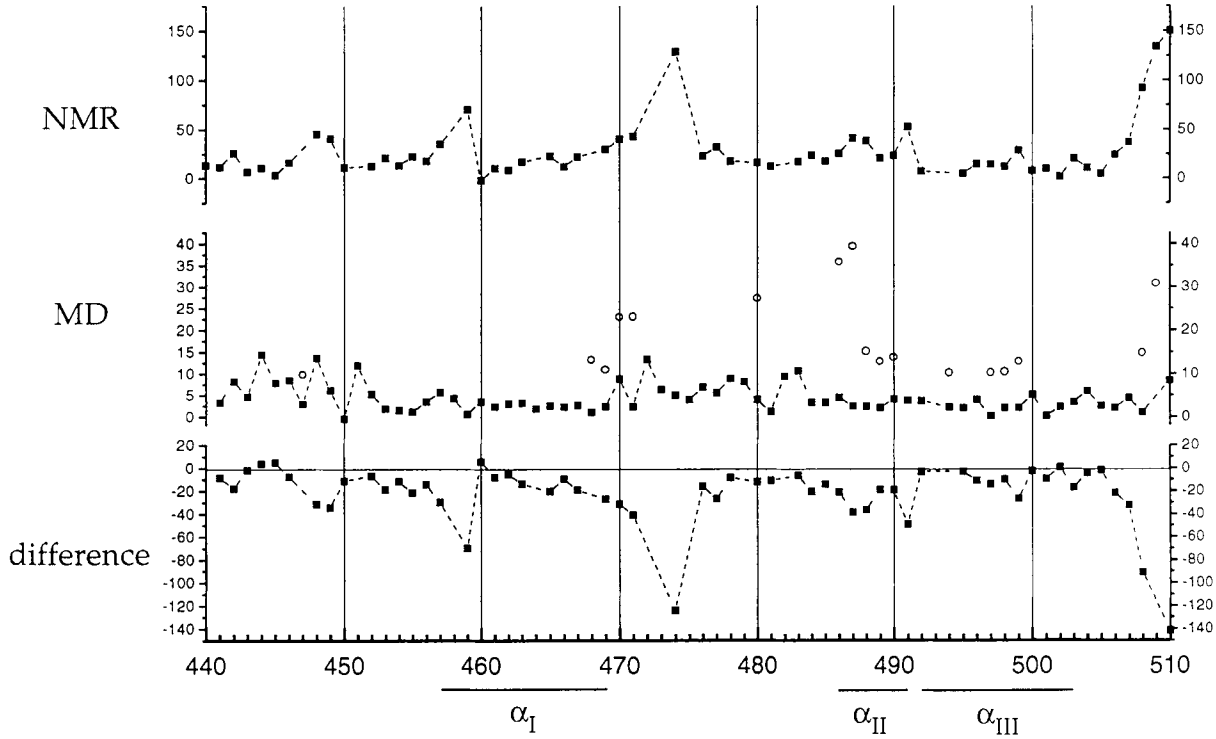

Fig. 9. Effective correlation times for the internal motions of the amide bonds (τ_e); **top,** experimental; **middle,** simulated; **bottom,** difference between simulated and experimental values. For better visualization, the relatively large error bars have been omitted. Note the different scales of the experimental and simulated τ_e-values.

thus in the same range as the simulated, the "model-free" approach[8] gives an adequate description of the motions they perform. On the other hand, for residues giving high differences in the τ_e-values, the MD simulation and the NMR experiment give information that complement each other: The simulation samples the first initial rapid decay with a possible perturbation from motions on a larger time scale, whereas the experiment, evaluated within the "model-free" model, gives information of larger scale motions, as indicated by the larger τ_e-values.

The jumps that were found in the simulation would thus be seen as a difference in the simulated and experimental τ_e-values. This is indeed true for Ile-487, and also for the residues Glu-470 and Gln-471 in the ext_I region, which are subject to other kinds of slower motions. It is possible to make a very rough estimate of the jump frequency of Ile-487–NH, between the charged oxygens of the side chain of Asp-485 ("site" i and j). Since $1/\tau_S = k_{ij} + k_{ji}$, where k_{ij} and k_{ji} are the rate constants for the jumps between the two sites,[5] and since we have assumed (see above) that $p_{eq}(i) = p_{eq}(j)$, this implies that $k_{ij} = k_{ji}$. The experimental τ_e-value for this residue was estimated to 41(±12) psec and the τ_e-value obtained from the simulation, when recalculating $C_{2i}(t)$ for shorter time periods (see above), was estimated to 1(±2) psec. This latter τ_e-value serves as an estimate of τ_f in Eq. (13). Since the total effective correlation time for the internal motion is independent of which model is used, integration of Eqs. (3) and (11) from $t = 0$ to ∞ yields:

$$\tau_e(1 - S^2) = \tau_f(1 - S_f^2) + \tau_s(S_f^2 - S^2) \quad (14)$$

and since $\tau_f << \tau_e$, τ_S can be expressed as

$$\tau_s = \frac{(1 - S^2)}{(S_f^2 - S^2)} \tau_e. \quad (15)$$

With estimates of S^2 and S^2_f from Table II, we obtain $\tau_S = 2.6\ \tau_e = 107$ (±32) psec. The jump frequency, k_{ij} will then be estimated to 4.6 (±2.0) $nsec^{-1}$ and in 200 psec the jump would occur 0.9 (±0.4) times. From Figure 6 it is clear that we have at least obtained the right order of magnitude of the jump frequency of Ile-487. It is more difficult to judge whether the jumps of Asp-485–O between Ser-444–NH and Arg-489–NH, found in the simulation, occur in reality or are an artifact of the simulation; τ_e for Ser-444–NH is in the same range in both the simulation and the experiment, whereas the experimental τ_e-values for Lys-486–NH and Arg-489–NH are about 20 psec higher than the simulated.

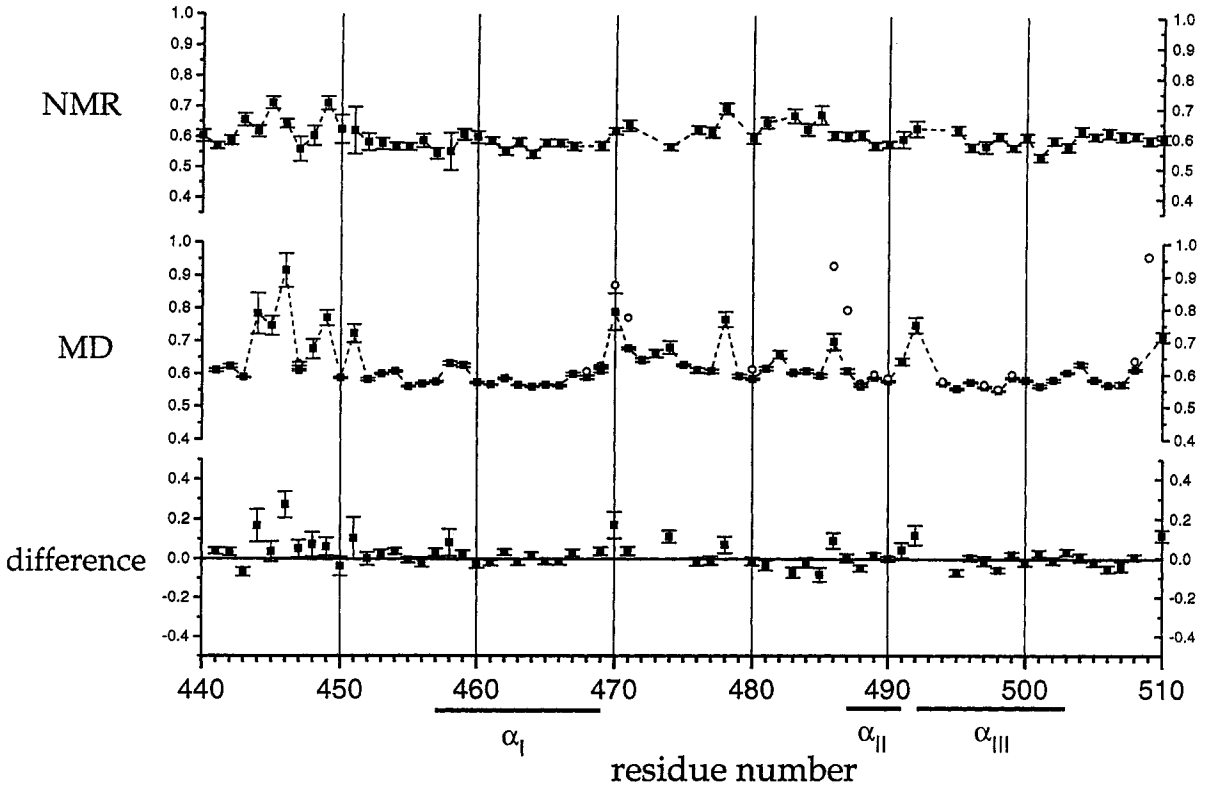

Fig. 10. T_1-values; **top,** experimental; **middle,** simulated; **bottom,** difference between simulated and experimental values.

{^{1}H}–^{15}N NOEs and T_1-Values

To be able to make a reasonable comparison between the experimental and simulated NOEs and T_1-values, we used the experimentally[4] estimated value of the overall rotation of the molecule, τ_R = 6.3 nsec in Eq. (7) to evaluate the simulated NOEs and T_1-values. The difference in the experimental and simulated order parameters (Fig. 2, bottom) will propagate as a corresponding (negative) difference in the T_1-values (Fig. 10, bottom).

The lower values (< 0.7) of the experimental {^{1}H}–^{15}N NOEs (Fig. 11, top), found in the middle of the Zn_I region and in the extended regions, could not be reproduced in the simulation (Fig. 11, middle), using a back calculation with the "model-free" model[8] (see Materials and Methods). Further, it is seen that the (negative) difference between simulated and experimental estimated τ_e-values (Fig. 9, bottom) correlates very well with, in the simulation, overestimated NOEs, i.e., residues with low NOEs will have larger τ_e-values. Since we are unable, for reasons discussed above, to sample these slower motions in the simulation, the simulated τ_e-values will result in overestimated and almost constant NOEs over the entire backbone of DBD.

The phenomenon is perhaps better understood when plotting NOE as a function of S^2 and τ_e with an overall rotational time of 6.3 nsec, using Eqs. (5)–(7) (Fig. 12, left). At the low (1–10 psec) τ_e-values acquired in the simulation, the NOEs are rather insensitive to the S^2-values (which also show a low variation along the protein backbone), explaining the monotonic values of the simulated NOEs. On the other hand, for τ_e-values around 100 psec, the NOEs are very sensitive to the generalized order parameter and a variation in the NOEs is thus to be expected if we were able to sample these slower motions, leading to larger τ_es in the simulation.

The T_1-values as a function of S^2 and τ_e (Fig. 12, right) also with τ_R = 6.3 nsec, using Eqs. (5) and (7), show quite a different behavior: First, the T_1-values are less sensitive to variations in τ_e (and S^2) and second, T_1 increases with decreasing S^2, whereas increasing τ_e instead decreases T_1. Moreover, in the S^2 range, where the underestimated order parameters are 0.5–0.7 (see Fig. 2, middle), the T_1-values are only weakly dependent on τ_e. This probably explains the high correlation between differences in simulated and experimental S^2- and T_1-values.

CONCLUSIONS

The uniform flexibility of the amide bonds throughout the backbone of GR DBD was seen for both the experimental and simulated order param-

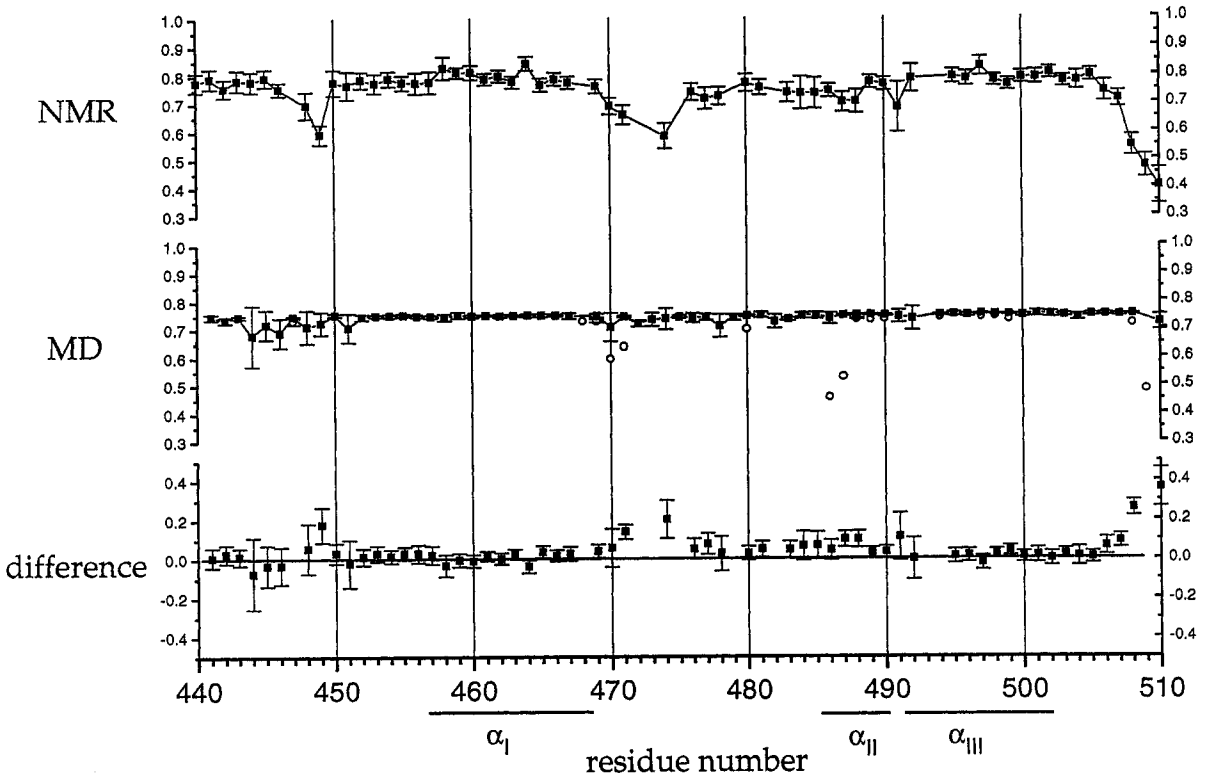

Fig. 11. {^{1}H}–^{15}N NOEs; **top,** experimental; **middle,** simulated; **bottom,** difference between simulated and experimental values.

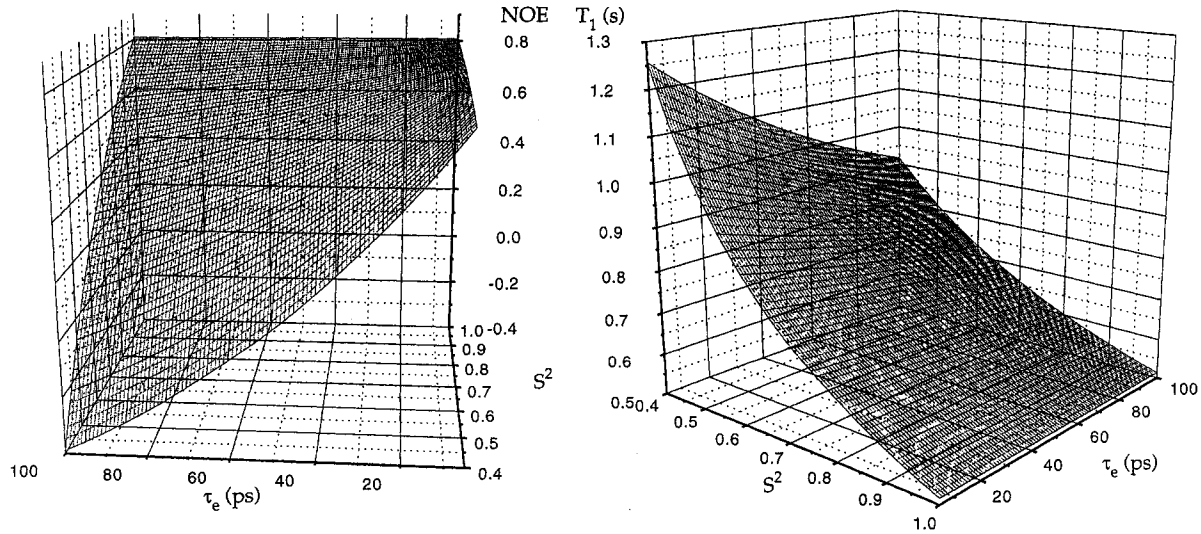

Fig. 12. {^{1}H}–^{15}N NOEs **(left)** and T_1-values **(right)** as a function of S^2 and τ_e (psec) with an overall rotational motion (τ_R) of 6.3 nsec calculated according to Eqs. (5)–(7).

eters. A somewhat reduced mobility was observed for the two major helices α_I and α_{III}, whereas the residues Cys-443 to Gly-449 in the Zn_I region might be more flexible.

The order parameter S^2 is a function of the average orientation of the amide bond and in cases where this average is poorly determined the S^2 value will be uncertain; it could be either too large or too small [see, for example, Eq. (13)]. Most of the order parameters that were underestimated in the

simulation and/or gave rise to a rapid decay of $C_{2i}(t)$ during the later part of the correlated time could be explained as (1) jumps of the amide proton (or the carbonyl oxygen of the preceding residue) between two preferred orientations that occurred only a few times during the simulation, resulting in a poor sampling of the two orientations. Such jumps were found for Asp-485–O between Ser-444–NH and Arg-489–NH, one of the N-terminal amide protons of Cys-440 between Asp-445–O and Glu-446–O and for Ile-487–NH between the charged oxygens of the side chain of Asp-485. (2) On the rapid motion of the amide bond is superimposed a larger scale motion which also will be poorly sampled in the relatively short simulation time. This could be the case for the residues Gly-470 and Gln-471, which are in the ext_I region of the protein and for the last residues of the C-terminal of the DBD fragment. These larger scale motions were also manifested as large differences in simulated and experimentally estimated τ_e-values; the latter were at least an order of magnitude larger for these residues. The information on a shorter time scale that can be obtained from an MD simulation thus complements the experimental information of the motions on a lower time scale, that cannot be sampled within the simulated time. By combining the experimental and simulated data and with use of an extended[35] form of the "model-free" model[8] it was possible to make rough estimates of the generalized order parameter S^2_S for the slower jumping motion and the jump frequency of Ile-487, between the charged oxygens of the side chain of Asp-485. It was further shown that NOEs lower than ~0.7 could not be reproduced in the simulation with a back calculation, using the "model-free" model, as a consequence of the shorter τ_e-values obtained from the simulation. Finally, it was shown that the T_1-values were almost independent of the τ_e-values in the S^2 range of DBD, with its relatively limited motions throughout the backbone, leading to a very high correlation between differences in simulated and experimental S^2- and T_1-values. Most of the residues, however, were not subject to any of the above described motions that could not be adequately sampled in the simulation, and in these cases the agreement between the experimental and simulated order parameters was as good as quantitative.

ACKNOWLEDGMENTS

We are grateful to Prof. Paul Sigler for providing coordinates for the crystal structure of the GR DBD–DNA complex. This work has been supported by the Swedish Natural Science Research Council (NFR).

REFERENCES

1. Kay, L.E., Dennis, A., Torchia, D.A., Bax, A. Backbone dynamics of proteins as studied by ^{15}N inverse detected heteronuclear NMR spectroscopy: Application to staphylococcal nuclease. Biochemistry 28:8972–8979, 1989.
2. Powers, R., Clore, G.M., Stahl, S.J., Wingfield, P.T., Gronenborn, A. Analysis of the backbone dynamics of the ribonuclease H domain of the human immunodeficiency virus reverse transcriptase using ^{15}N relaxation measurements. Biochemistry 31:9150–9157, 1992.
3. Kördel, J., Skelton, N.J., Akke, M., Palmer III, A.G., Chazin, W.J. Backbone dynamics of calcium-loaded calbindin D_{9k} studied by two-dimensional proton-detected ^{15}N NMR spectroscopy Biochemistry 31:4856–4866, 1992.
4. Berglund, H., Kovács, H., Dahlman-Wright, K., Gustafsson, J.-Å, Härd, T. Backbone dynamics of the glucocorticoid receptor DNA-binding domain. Biochemistry 31: 12001–12011, 1992.
5. Clore, G.M., Driscoll, P.C., Wingfield, P.T., Gronenborn, A.M. Analysis of the backbone dynamics of interleukin-1β using two-dimensional inverse detected heteronuclear ^{15}N-^{1}H NMR spectroscopy. Biochemistry 29:7387–7401, 1990.
6. Schneider D.M., Dellwo M.J., Wand A.J. Fast internal main-chain dynamics of human ubiquitin. Biochemistry 31:3645–3652, 1992.
7. Peng, J.W., Wagner, G. Mapping of spectral density functions using heteronuclear NMR relaxation measurements. J. Magn. Reson. 98:308–332, 1992.
8. Lipari, G., Szabo, A. Model-free approach to the interpretation of nuclear magnetic resonance relaxation in macromolecules. 1. Theory and range of validity. J. Am. Chem. Soc. 104:4546–4559, 1982.
9. Clore, G.M., Szabo, A., Bax, A., Kay, L.E., Driscoll, P.C. Gronenborn, A.M. Deviation from the simple two-parameter model-free approach to the interpretation of nitrogen-15 nuclear magnetic relaxation of proteins. J. Am. Chem. Soc. 112:4989–4991, 1990.
10. Chandrasekhar, I., Clore, G.M., Szabo, A., Gronenborn, A.M., Brooks, B.R. A 500 ps molecular dynamics simulation of interleukin-1β in water. Correlation with nuclear magnetic resonance spectroscopy and crystallography. J. Mol. Biol. 226:239–250, 1992.
11. Kördel, J., Teleman, O. Backbone dynamics of calbindin D_{9K}: Comparison of molecular dynamics simulations and ^{15}N NMR relaxation measurements. J. Am. Chem. Soc. 114:4934–4936, 1992.
12. Härd, T., Kellenbach, E., Boelens, R., Kaptein, R., Dahlman, K., Carlstedt-Duke, J., Freedman, L.P., Maler, B.A., Hyde, E.I., Gustafsson, J.-Å, Yamamoto, K.R. ^{1}H NMR studies of the glucocorticoid receptor DNA-binding domain: Sequential assignments and identification of secondary structure elements. Biochemistry 29:9015–9023, 1990.
13. Härd, T., Kellenbach, E., Boelens, R., Maler, B.A., Dahlman, K., Freedman, L.P., Carlstedt-Duke, J., Yamamoto, K.R., Gustavsson, J.Å., Kaptein R. Solution structure of the glucocorticoid receptor DNA-binding domain. Science 249:157–160, 1990.
14. Luisi, B.F., Xu, W.X., Otwinowski, Z., Freedman, L.P., Yamamoto, K.R., Sigler, P.B. Crystallographic analysis of the interaction of the glucocorticoid receptor with DNA. Nature (London) 352:497–505, 1991.
15. Danielsen, M., Hinck, L., Ringold, G. Two amino acids within the knuckle of the first zinc finger specify DNA response element activation by the glucocorticoid receptor. Cell 57:1131–1138, 1989.
16. Mader, S., Kumar, V., de Verneuil, H., Chambon, P. Three amino acids of the oestrogen receptor are essential to its ability to distinguish an oestrogen from a glucocorticoid responsive element. Nature (London) 338:271–274, 1989.
17. Umesuno, K., Evans, R.M. Determinants of target gene specificity for steroid/thyroid hormone receptors. Cell 57: 1139–1146, 1989.
18. Schwabe, J.W.R., Neuhaus, D., Rhodes, D. Solution structure of the DNA-binding domain of the oestrogen receptor. Nature (London) 348:458–461, 1990.
19. Levy, R.M., Karplus, M. Increase of ^{13}C NMR relaxation times in proteins due to picosecond motional averaging. J. Am. Chem. Soc. 4:994–996, 1981.
20. Abragam, A. In: "The Principles of Nuclear Magnetism." Oxford, England: Clarendon Press, 1961: 289–316.
21. Hiyama, Y., Niu, C., Silverton J.V., Bavoso, A., Torchia, D.A. Determination of ^{15}N chemical shift tensor via ^{15}N-^{2}H dipolar coupling in BOC-glycylglycyl[^{15}N] glycine benzyl ester. J. Am. Chem. Soc. 110:2378–2383, 1988.

22. Eriksson M.A.L., Härd T., Nilsson L. To be published.
23. Brooks, B.R., Bruccoleri, R.E., Olafsen, B.D., States, D.J., Swaminathan, S., Karplus M. CHARMM: A program for macromolecular energy, minimization and dynamics calculations. J. Comput. Chem. 4:187–217, 1983.
24. Dewar, M.J.S., Thiel, W. J. Ground states of molecules. 38. The MNDO method. Approximation and parameters. J. Am. Chem. Soc. 99:4899–4906, 1977.
25. Dewar, M.J.S., Thiel, W. J. Ground states of molecules. 39. MNDO results for molecules containing hydrogen, carbon, nitrogen and oxygen. J. Am. Chem. Soc. 99:4907–4917, 1977.
26. Dewar, M.J.S., Merz K.M., Jr. MNDO calculations for compounds containing zinc. Organometallics 5:1494–1496, 1986.
27. Besler, B.H., Merz, K.M., Jr., Kollman, P.A. Atomic charges derived from semiempirical methods. J. Comp. Chem. 11: 431–439, 1990.
28. Steward, J.J.P. MOPAC: A semiempirical molecular orbital program. J. Comput. Aided Mol. Design 4:1–45, 1990.
29. Brünger, A., Karplus M. Polar hydrogen positions in proteins: Empirical energy placement and neutron diffraction comparison. Proteins 4:148–156, 1988.
30. Jorgensen, W.L., Chandraseklar, J., Madura, J.D., Impey, R.W., Klein, M.L. Comparison of simple potential functions for simulating liquid water. J. Chem. Phys. 79:926–935, 1983.
31. Berkowitz, M., Mc. Cammon, J.A. Molecular dynamics with stochastic boundary conditions. Chem. Phys. Lett. 90: 215–217, 1982.
32. Brooks, C.L., III, Karplus, M. Deformable stochastic boundaries in molecular dynamics. J. Chem. Phys. 79: 6312–6325, 1983.
33. Ryckaert, J.P., Ciccotti, G., Berendsen, H.J.C. Numerical integration of the Cartesian equations of motion of a system with constraints: Molecular dynamics of n-Alkanes. J. Comp. Phys. 23:327–341, 1977.
34. Creighton, T. In: "Proteins, Structures and Molecular Properties." New York: W.H. Freeman, 1984: 5–6.
35. Wittebort, R.J., Szabo, A. Theory of NMR relaxation in macromolecules: Restricted diffusion and jump models for multiple internal rotations in amino acid side chains. J. Chem. Phys. 69:1722–1736, 1978.
36. Kraulis, P.J. MOLSCRIPT: A program to produce both detailed and schematic plots of protein structures. J. Appl. Crystallogr. 24:946–950, 1991.